11th World Congress on Structural and Multidisciplinary Optimization
7th - 12th, June 2015, Sydney Australia

Optimizing Topology Optimization with Anisotropic Mesh Adaptation

Kristian E. Jensen[1]

[1] Imperial College London, SW7 2AZ London, United Kingdom, kristianejlebjerg@gmail.com

1. Abstract
Mesh adaptation is rarely used in topology optimisation, with exceptions found in continuous methods such as phase field and some level-set techniques. Anisotropic mesh adaptation involve not only refinement and coarsening operations, but also smoothing and swapping, which allow for the appearance of elongated elements aligned with physical features, such as those found in structural optimisation. We use an anisotropic mesh generator based on local mesh modifications and an open source finite element engine (FEniCS) in combination with the method of moving asymptotes. Discrete sensitivities are calculated automatically and converted to continuous ones, such that they can drive the mesh adaptation and be interpolated between meshes. Results for stress and compliance constrained volume minimisation indicate that mesh independence is possible in a rounded 2D L-bracket geometry, the rounding fillet being 1 % of the characteristic length scale. Finally, the combination is tested for 3D compliance minimisation, where 50 is found to be a typical average element aspect ratio, indicative of the speed-up relative to isotropic mesh adaptation.
2. Keywords: Anisotropic; mesh; adaptation; topology; optimization

3. Introduction
Fixed structured meshes remain popular for topology optimisation due to ease of implementation and parallelisation [1, 2]. Adapted meshes have, however, also seen some use in the context of continuous sensitivities [3, 4] and recently also for discrete sensitivities [5], but we are not aware of any work employing mesh adaptation of the anisotropic kind, which is the aim of this work. The hypothesis is that stretching of elements to accommodate anisotropic features in the design and the physics will enable a more efficient use of computational resources compared to isotropic mesh adaptation.

4. Anisotropic Mesh Adaptation
We choose to apply a continuous framework [6] for anisotropic mesh adaptation. That is, we estimate the optimal local size and orientation of elements by means of a spatially varying symmetric positive definite tensor field, a metric tensor field, $\mathcal{M}$. If one wishes to minimise the interpolation error of some scalar, $\tilde{\rho}$, then the metric is [7]

$$\underline{\underline{\mathcal{M}}} = \frac{1}{\eta}\left(\det[\underline{\underline{\text{abs}}}(\underline{\underline{\mathbf{H}}}(\tilde{\rho}))]\right)^{-\frac{1}{2q+d}} \underline{\underline{\text{abs}}}(\underline{\underline{\mathbf{H}}}(\tilde{\rho})), \tag{1}$$

where $\det(\cdots)$ returns the determinant, $\underline{\underline{\mathbf{H}}}(\cdots)$, returns the Hessian, $\underline{\underline{\text{abs}}}(\cdots)$ takes the absolute value of the tensor in the principal frame, q is the error norm to be minimised, d is the dimension and finally, η is a scaling factor used to control the number of elements. Several metrics can be combined using the inner ellipse method [8] illustrated in figure 1, where it can also be seen that the metric has units of inverse squared length. The metric can be used

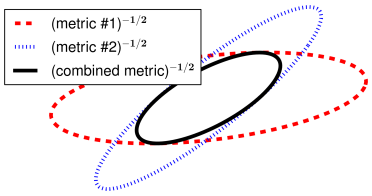

Figure 1: The process of combining two metrics using the inner ellipse method is shown for the case where there is an intersection and thus also a loss of anisotropy, but anisotropy is preserved whenever one ellipse is entirely within the other.

to map elements to metric space, where the ideal elements are regular triangles or tetrahedra. Various heuristic quality metrics exists to quantify the difference from the perfect element [9]. These metrics are generally invariant

under rotations in metric space, which can give rise to large angles in real space and thus also problems with iterative solvers. This is, however, mostly an issue for extreme aspect ratio elements, and it is possible to reduce the occurrence of large angles with advancing front techniques [10]. We use a popular technique [8, 11] based on the local mesh modifications shown in figure 2. The results presented here are based on an Octave/MATLAB implementation, which is fully vectorised. It is, however, still around an order of magnitude slower than an equivalent C++ implementation [12].

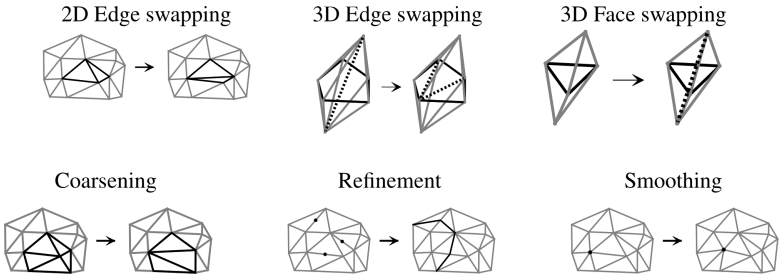

Figure 2: Local swapping mesh modification operations are illustrated in two and three dimensions (top row), while coarsening, refinement and smoothing are sketched for two dimensions. Smoothing and swapping operations are only allowed, when they improve the worst local element quality, and in three dimensions this is also true for the refinement.

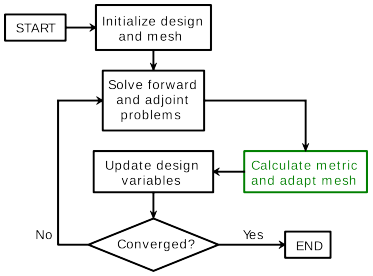

Figure 3: The flowchart for a optimisation is sketched with the mesh adaptation between the sensitivity analysis and the optimiser.

5. Topology Optimisation

We use the standard approach of Solid Isotropic Material with Penalisation (SIMP) [13] together with the method of moving asymptotes [14],

$$E = E_{\min} + (E_{max} - E_{\min})\rho^{P_E}, \quad \text{where} \quad 0 \leq \rho \leq 1, \tag{2}$$

where E is the Young's modulus, ρ is the design variable and P_E is the SIMP penalisation exponent. For compliance minimisation, $P_E = 1$ gives rise to a convex problem, which does not have a discrete solution. Its solution, however, constitutes a good initial guess for an optimisation with larger P_E, where the optimal solution is discrete. This kind of continuation approach is common for addressing problems with local minima within the field of structural optimisation [15].

We calculate the discrete sensitivity with respect to the design variables automatically [16], and then normalise the sensitivity with the design variable volumes to calculate an approximate continuous sensitivity, ∂_ρ. To this, we apply Helmholtz smoothing [17], such as to impose a minimum length scale, $L_{\min}$,

$$\partial_\rho - \tilde{\partial}_\rho + L_{\min}^2 \nabla^2 \tilde{\partial}_\rho = 0. \tag{3}$$

The filter is also applied on the design variable and both scalar fields are then used to calculate metrics using equation (1). The metrics are combined using the inner ellipse method, and the result is passed to the mesh generator. The filtered continuous sensitivities, mma asymptotes as well as current, old and older design variables are interpolate on to the new mesh. The discrete sensitivity on the new mesh is estimate by multiplying with the new design variable volumes, and then design variables are optimised completing the optimisation loop sketched in figure 3.

We use an open source high level finite element package [18] (FEniCS) for solving the forward problem. Both displacements and design variable are represented with continuous linear basis functions. The Hessian calculation in equation (1) involves Galerkin projection and these are performed with an iterative solver, but a direct solver is applied for the forward, adjoint and filter problems.

6. Setup

We show results in the context of linear elasticity in three dimensions as well as for plane stress, but in both cases we use $E_{\max}$ and a characteristic length, L_{char} to non-dimensionalise the problem,

$$\nu = 0.3, \quad E_{\min} = 10^{-3} E_{\max}, \quad L_1 = 0.1 L_{\text{char}}, \quad \underline{\underline{\sigma}}_{\text{load}} = E_{\max}/L_{\text{char}}, \quad q = 2 \quad \text{and} \quad c_{\text{MMA}} = 10^3,$$

where ν is the Poisson ratio, L_1 is a length scale associated with the load boundary condition and c_{MMA} is the MMA c parameter for controlling the enforcement of constraints. We also use move limits

$$\text{abs}(\rho_{i+1} - \rho_i) = \Delta\rho,$$

and we fix these at $\Delta\rho = 0.1$.

6.1 Stress and compliance constrained volume minimisation in two dimensions
This setup is specific to a L-bracket geometry with a rounded corner (fillet 1% of the characteristic length scale). For these optimisations, we use a stress penalisation scheme [19] to avoid problems with void stress, and we use a 10-norm to convert the local constraints to a single global one [20]. We also smooth the stress sensitivity with a Helmholtz filter based on the element metric calculated as Steiner ellipses and use a factor of four higher tolerance for the metric associated with the stress sensitivity. We scale the number of iterations with the mesh tolerance:

$$\text{it}_{\max} = \text{round}(600\sqrt{0.02/\eta_{\tilde{\rho}}}), \quad C_{\max} = 2.5E_{\max}L_{\text{char}}^2, \quad \sigma_{\max} = 1.5E_{\max}, \quad P_E = 3 \quad \text{and} \quad L_{\min} = 5\cdot 10^{-2}L_{\text{char}},$$

where $C_{\max}$ and $\sigma_{\max}$ is the maximum compliance and von misses stress, respectively.

6.2 Volume constrained compliance minimisation in three dimensions
The implementation is tested for a cantilever, stool and crank geometry, which correspond to bending, compression and torsion, respectively. The tests are described as part of another work [21]. We use volume fractions of 10 %, 20 % and 50 %, minimum length scales of $5\cdot 10^{-3}$, $1\cdot 10^{-2}$ and $1\cdot 10^{-2}$, respectively. Convergence is investigated for the cantilever, but mesh tolerances for the stool and crank are fixed at 0.04 and 0.02. We use as much symmetry as possible and fix the maximum number of iterations at $\text{it}_{\max} = 300$. To reduce issues with local minima, the SIMP exponent is increased exponentially throughout the first 2/3rds of the optimisation

$$P_E^i = \min(4^{3i/(2\text{it}_{\max})}, 4).$$

7. Results
Due to the inconsistent formulation of our approach, we do not expect convergence in a strict sense and thus plot the best results satisfying the constraints to the tolerance of the MMA c parameter*.
The two dimensional results are shown in figure 4 with the volume throughout the optimisations plotted in figure 5(a). Both the topology and objective function seems to converge, which was not the case for a sharp corner. The maximum von misses stress is twice the allowed value underlining the need for post processing of designs obtained with stress constrained topology optimisation. We attribute the fact that the volume and compliance in figure 5 converge from above to the continuous design variables, that is the area of intermediate, and thus suboptimal design, is reduced with mesh refinement. The opposite behaviour would be expected, if the convergence of the forward problem was the dominating effect.
The compliance for the three dimensional results is plotted in figure 5(b) with the actual designs shown in figures 6 and 7 by means of $\rho = 0.5$ iso-surfaces and slices at constant x. Note that these representations can produce quadrilaterals from purely tetrahedral meshes, and that the blue wireframe represents the computational domain in which objective function and node count are calculated, see top of each design. All designs agree with a previous work [21] and in the case of the cantilever we get convergence of topology as well as objective function, but we did find a different topology, if the cantilever was optimised with $L_{\min} = 5\cdot 10^{-2}$. The oscillations for the objective functions plotted in figure 5(b) seem stronger than for the two dimensional case, but the absence of a stress constraint seems to improve the ability to recover from infeasible designs.

7.1 Computational cost
The computational time in hours† is printed above the designs in figures 4, 6 and 7. An estimate for the aspect ratio (AR) is also printed for the three dimensional results. This is calculated by first computing the Steiner ellipsoid and then dividing the product of the radii with the cubed minimum radii. The aspect ratio can be used as an estimate of speed-up relative to isotropic adaptation and it seems to vary with mesh resolution, but values below 50 are rare. One can make an equivalent analysis for the two-dimensional results and arrive at 4-5, but as seen from figures 4, 6 and 7, it also depends on the problem.
The mesh adaptation takes up 20-30 % of the total computational time for the two dimensional results and 40-50 % in three dimensions. This is with single threaded computations, a direct solver and an Octave/MATLAB implementation for the mesh adaptation, so it might be possible to decrease the total computational time with an order of magnitude, by employing an optimised C++ mesh adaptation implementation [12] in combination with an iterative solver. In this regard, the influence of elements with large angles would be particularly interesting.

*In three dimensions we use $c_{\text{mma}} = 10^3$, but show designs satisfying the constraints to within 0.5%
†Using an Intel(R) Core(TM) i7 870 @ 2.93GHz, everything being run single threaded

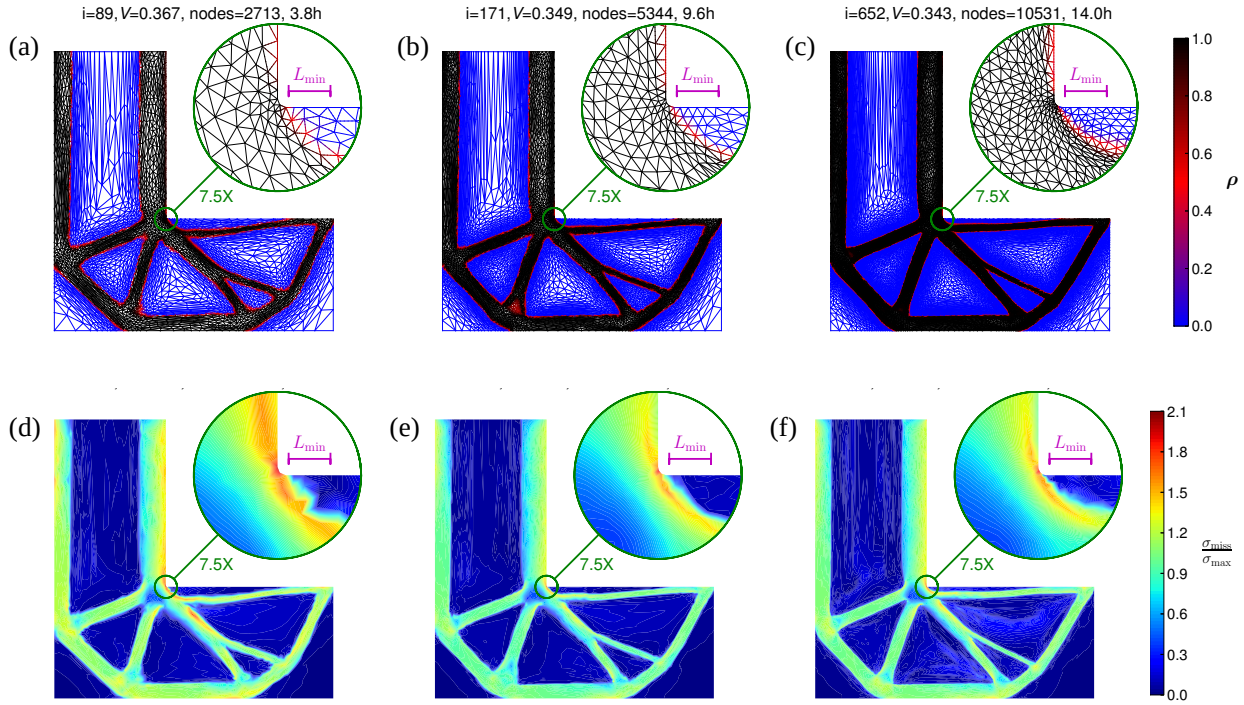

Figure 4: Optimisations with a rounded corner for $\eta_{\tilde{\rho}}$ equal to 0.03 (left), 0.015 (middle) and 0.0075 (right). The design variables and mesh elements are shown for the iteration (i) at which the lowest volume fraction (V) occurs, while the stress and compliance constraints are satisfied. The designs are shown in the upper row (a-c) with the von misses stress below (d-e).

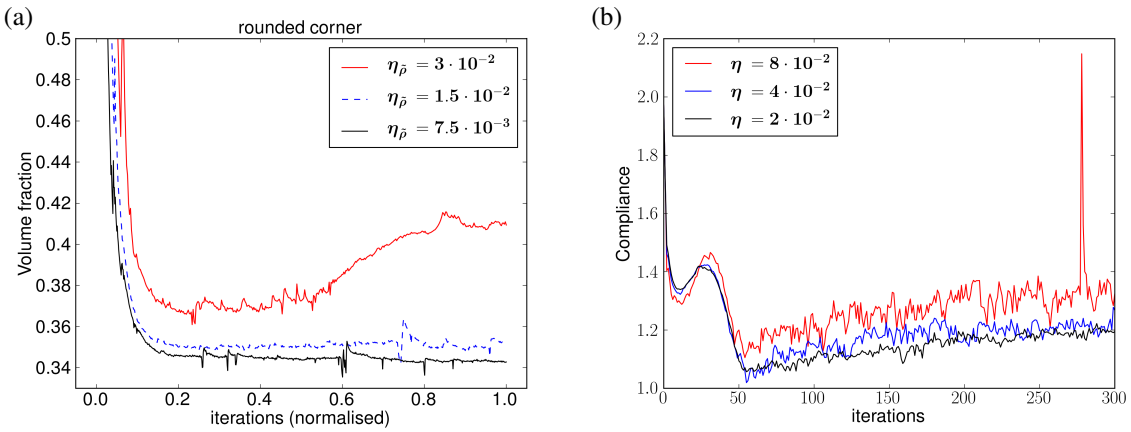

Figure 5: The volumes of optimisations for a stress and compliance constrained L-bracket problem is plotted to the left (a), while the compliance for a volume constrained three dimensional cantilever problem is plotted to the right (b). In both cases three different values for the tolerances of the mesh adaptation is shown. Note how the coarse stress constrained optimisation becomes infeasible and fails to recover. The spike of the coarse three dimensional could also be due to infeasible designs. For the three dimensional problems, the P_E parameter is smaller than 4 before iteration 200.

8. Conclusion

We have combined topology optimisation with anisotropic mesh adaptation and tested the implementation on stress and compliance constrained volume minimisation for the two dimensional L-bracket problem with a ever so slightly rounded corner as well as on volume constrained compliance minimisation in three dimensions. In both cases we are able to get mesh independence for the topology and convergence of the objective function.

9. Acknowledgement
This is work supported by the Villum Foundation.

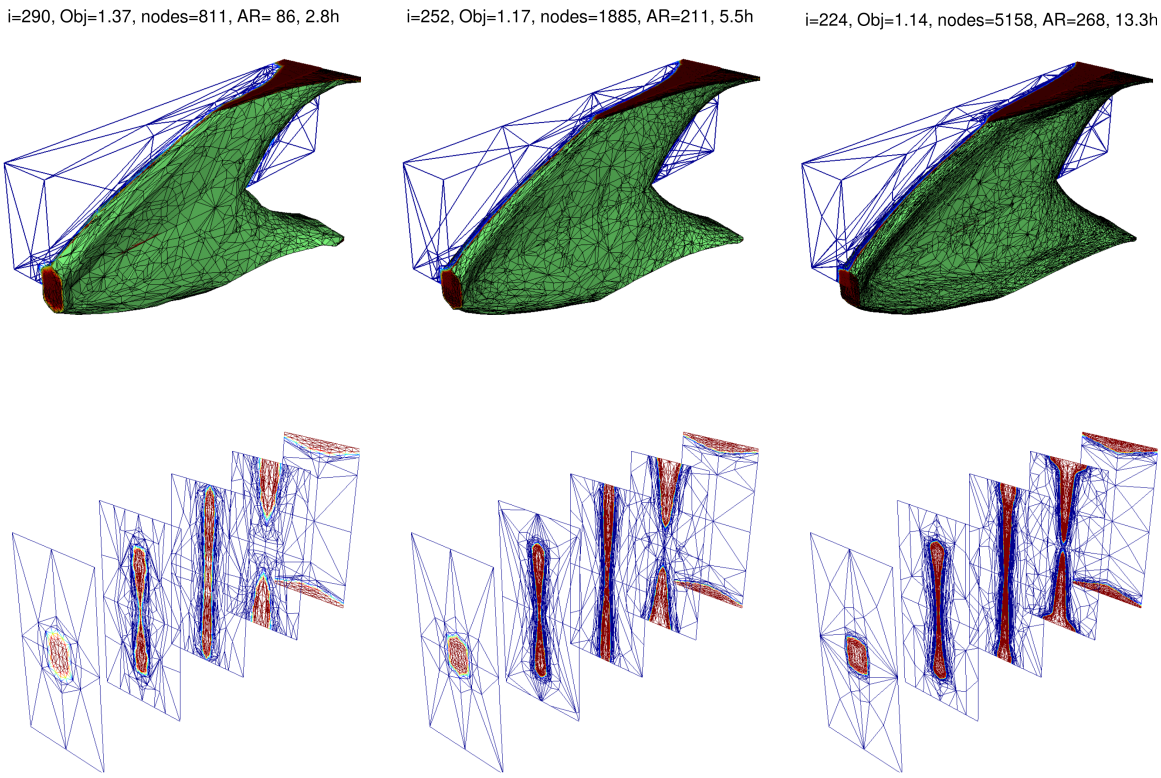

Figure 6: The best cantilever designs that satisfy the volume constraint to a relative tolerance of 0.5% are shown in terms of the $\rho = 0.5$ isosurfaces as well as slices at x/L_y equal to 0, 0.25, 0.5, 0.75 and 1. They all give the same topology, but the slice through $x = 0.25L_y$ shows significant variations.

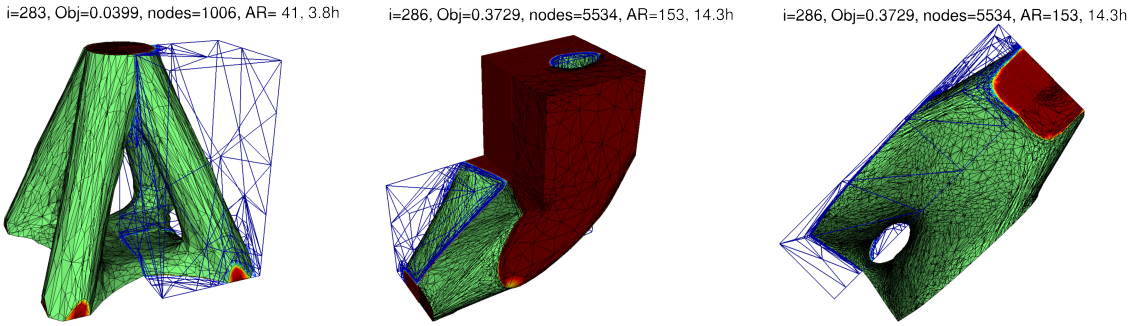

Figure 7: The best stool (left) and crank (center, right) designs are plotted in terms of their $\rho = 0.5$ isosurfaces. The crank shown from the side (center) with the support visible and from the bottom where the load is applied (right). Note that the title statistics pertain to the actual computational domain as illustrated with the blue wireframe.

10. References

[1] Erik Andreassen, Anders Clausen, Mattias Schevenels, Boyan S Lazarov, and Ole Sigmund. Efficient topology optimization in matlab using 88 lines of code. *Structural and Multidisciplinary Optimization*, 43(1):1–16, 2011.

[2] Niels Aage, Erik Andreassen, and Boyan Stefanov Lazarov. Topology optimization using petsc. *Structural and Multidisciplinary Optimization*, 2015.

[3] Mathias Wallin, Matti Ristinmaa, and Henrik Askfelt. Optimal topologies derived from a phase-field method. *Structural and Multidisciplinary Optimization*, 45(2):171–183, 2012.

[4] Samuel Amstutz and Antonio A Novotny. Topological optimization of structures subject to von mises stress constraints. *Structural and Multidisciplinary Optimization*, 41(3):407–420, 2010.

[5] Asger Nyman Christiansen, J Andreas Bærentzen, Morten Nobel-Jørgensen, Niels Aage, and Ole Sigmund. Combined shape and topology optimization of 3d structures. *Computers & Graphics*, 46:25–35, 2015.

[6] Adrien Loseille and Frédéric Alauzet. Continuous mesh framework part i: well-posed continuous interpolation error. *SIAM Journal on Numerical Analysis*, 49(1):38–60, 2011.

[7] Long Chen, Pengtao Sun, and Jinchao Xu. Optimal anisotropic meshes for minimizing interpolation errors in $\mathscr{L}^p$-norm. *Mathematics of Computation*, 76(257):179–204, 2007.

[8] CC Pain, AP Umpleby, CRE De Oliveira, and AJH Goddard. Tetrahedral mesh optimisation and adaptivity for steady-state and transient finite element calculations. *Computer Methods in Applied Mechanics and Engineering*, 190(29):3771–3796, 2001.

[9] Yu V Vasilevski and KN Lipnikov. Error bounds for controllable adaptive algorithms based on a hessian recovery. *Computational Mathematics and Mathematical Physics*, 45(8):1374–1384, 2005.

[10] Adrien Loseille. Metric-orthogonal anisotropic mesh generation. *Procedia Engineering*, 82:403–415, 2014.

[11] Xiangrong Li, Mark S Shephard, and Mark W Beall. 3d anisotropic mesh adaptation by mesh modification. *Computer methods in applied mechanics and engineering*, 194(48):4915–4950, 2005.

[12] Georgios Rokos, Gerard J Gorman, James Southern, and Paul HJ Kelly. A thread-parallel algorithm for anisotropic mesh adaptation. *arXiv preprint arXiv:1308.2480*, 2013.

[13] Martin Philip Bendsoe and Ole Sigmund. *Topology optimization: theory, methods and applications*. Springer, 2003.

[14] Krister Svanberg. The method of moving asymptotesa new method for structural optimization. *International journal for numerical methods in engineering*, 24(2):359–373, 1987.

[15] Albert A Groenwold and LFP Etman. A quadratic approximation for structural topology optimization. *International Journal for Numerical Methods in Engineering*, 82(4):505–524, 2010.

[16] Patrick E Farrell, David A Ham, Simon W Funke, and Marie E Rognes. Automated derivation of the adjoint of high-level transient finite element programs. *SIAM Journal on Scientific Computing*, 35(4):C369–C393, 2013.

[17] Boyan Stefanov Lazarov and Ole Sigmund. Filters in topology optimization based on helmholtz-type differential equations. *International Journal for Numerical Methods in Engineering*, 86(6):765–781, 2011.

[18] Anders Logg, Kent-Andre Mardal, Garth N. Wells, et al. *Automated Solution of Differential Equations by the Finite Element Method*. Springer, 2012.

[19] GD Cheng and Xiao Guo. ε-relaxed approach in structural topology optimization. *Structural Optimization*, 13(4):258–266, 1997.

[20] Pierre Duysinx and Ole Sigmund. New developments in handling stress constraints in optimal material distribution. In *Proc of the 7th AIAA/USAF/NASAISSMO Symp on Multidisciplinary Analysis and Optimization*, volume 1, pages 1501–1509, 1998.

[21] Thomas Borrvall and Joakim Petersson. Large-scale topology optimization in 3d using parallel computing. *Computer methods in applied mechanics and engineering*, 190(46):6201–6229, 2001.